Single molecule analysis reveals positive allosteric modulators are required to stabilize the active state of a metabotropic glutamate receptor

Anne-Marinette Cao[1*†], Robert B. Quast[1*], Fataneh Fatemi[1,3], Philippe Rondard[2], Jean-Philippe Pin[2,#], Emmanuel Margeat[1,#]

[1] *Centre de Biologie Structurale (CBS), Univ. Montpellier, CNRS, INSERM, Montpellier, France*

[2] *Institut de Génomique Fonctionnelle, Univ. Montpellier, CNRS, INSERM, 141 rue de la Cardonille, 34094, Montpellier Cedex 05*

[3] *Protein Research Center, Shahid Beheshti University, Shahid Beheshti University, Tehran, Iran*

* These authors contributed equally to this work.

: Corresponding authors : jean-philippe.pin@igf.cnrs.fr, margeat@cbs.cnrs.fr

† Present address: École Polytechnique Fédérale de Lausanne (EPFL), SB ISIC LCBM, Station 6, 1015 Lausanne, Switzerland

AUTHOR CONTRIBUTIONS:

Anne-Marinette Cao: Detergent screening, protein preparation and purification, preliminary LRET and smFRET experiments, revised the manuscript

Robert B. Quast: Detergent optimization, protein preparation and purification, LRET and smFRET data acquisition and analysis, wrote the manuscript

Fataneh Fatemi: Preliminary protein preparation and purification and smFRET experiments, revised the manuscript

Philippe Rondard: Experiment design, data interpretation, revised the manuscript.

Jean-Philippe Pin: Experiment design, data interpretation, acquisition of funds, revised the manuscript

Emmanuel Margeat: Experimental design, data analysis and interpretation, design and implementation of the smFRET setup, acquisition of funds, wrote the manuscript

Abstract

Metabotropic glutamate receptors (mGlu) are G protein-coupled receptors that represent promising targets for brain diseases. Much hope in drug development come from the discovery of positive allosteric modulators that display subtype selectivity, and act by increasing agonist potency, as well as efficacy in most cases. How such compounds can influence agonist efficacy remains unclear. Here, we explore the structural dynamics of the full-length mGlu2 dimers at submillisecond timescales using single molecule FRET on diffusing receptors in optimized detergent micelles. We show that glutamate binding in the Venus flytrap extracellular domains does not stabilize fully the receptors in their active states. The full activation of all receptors can only be observed in the presence of either a positive allosteric modulator or the Gi protein. Our results provide important new insights on the fast kinetics and the action of the allosteric modulators on mGlu activation at the single molecule level.

Introduction

G protein-coupled receptors (GPCR) constitute the largest superfamily of integral membrane receptors encoded in the human genome and are involved in various physiological processes (Lagerström and Schiöth 2008). All GPCRs share the common structural motif of 7 transmembrane-spanning mostly α-helical segments (7TM) that mediate the transmission of external signals, mainly provided in the form of ligands, into the interior of cells(Hilger, Masureel, and Kobilka 2018; García-Nafría and Tate 2019). In contrast to the classical idea of ligand-induced conformational transitions from inactive to active states, accumulating evidence show that GPCRs continuously oscillate between multiple conformations either in unliganded or ligand-bound states (Latorraca, Venkatakrishnan, and Dror 2017; Weis and Kobilka 2018). However, a structural understanding of the underlying mechanisms of receptor activation is complicated by the conformational heterogeneity within ensembles of molecules, making it difficult to identify the totality of visited individual conformational states.

The conformational dynamics governing metabotropic glutamate receptor (mGlu) activation have been described to occur at microsecond to millisecond timescales(Marcaggi et al. 2009; Grushevskyi et al. 2019; Hlavackova et al. 2012). These are prototypical class C GPCRs, comprising an extended N-terminal extracellular domain (ECD) involved in ligand-binding and dimerization (Pin and Bettler 2016; Niswender and Conn 2010). This ECD includes a Venus-flytrap domain (VFT), bearing the orthosteric ligand binding site, and a cysteine-rich domain (CRD), which links the VFT to the 7TM (Figure 1a). As a result of this multidomain architecture the orthosteric ligand-binding site is separated from the site of transducer activation by more than 10 nm. Therefore, the transmission

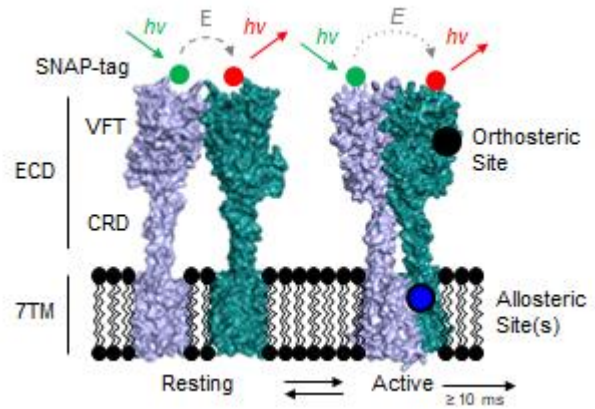

Figure 1: Structure and conformational rearrangements of mGlu. Structural model of dimeric mGlu2 in resting and active conformations. The major structural elements of each subunit include the extracellular domain (ECD), comprising the venus fly-trap domain (VFT), the cysteine rich domain (CRD), and the seven transmembrane domain (7TM). Activation leads to a closure of the VFTs and a reorientation of the ECDs, the CRDs and the 7TMs. This leads to a decrease of the FRET efficiency between the two dyes at the N-terminus. The shown structures were obtained by homology modeling using mGlu5 structures PDB ID 6N52 and 6N51.

of external signals, mediated by multiple correlated conformational domain rearrangements, requires a precise allosteric interdomain and intersubunit communication to achieve such a long-range functional link. Our understanding of the major conformational rearrangements has recently been substantiated by high-resolution structures of mGlu1 and mGlu5 that show i) reorientation of the ECDs, ii) closure of the upper and lower lobes of the VFT, iii) inward movement of the CRD and iv) reorientation of the 7TMs, altogether bringing the two receptor subunits into closer proximity (Figure 1)(Koehl et al. 2019; Zhang et al. 2020).

Conformational dynamics of mGlu have recently been studied by us and others using ensemble and single molecule Förster resonance energy transfer (smFRET), but the impact of G protein and allosteric ligands that bind to their 7TM is still lacking. Our work in isolated ECDs pointed at an activation mechanism that is governed by a shift in the equilibrium between preexisting conformational states, with the existence of a dominant population rapidly oscillating between active and resting states at submillisecond timescales(Olofsson et al. 2014). A study on full-length, surface-immobilized receptor dimers confirmed the dynamic nature of the VFT, although the experimental time resolution did not allow addressing the rapid dynamics seen on isolated VFTs(Vafabakhsh, Levitz, and Isacoff 2015). In a recent ensemble FRET approach, performed on fluorescent protein-engineered receptor dimers, the idea of microseconf (µs) to millisecond (ms) structural dynamics governing mGluR activation was further substantiated(Grushevskyi et al. 2019).

In order to understand the mechanistic principles and the role of fast dynamics in the initial steps of mGluR2 activation, we combine in the present study a careful preparation of receptors under

conditions retaining their functional integrity over prolonged periods of time, with the ability offered by diffusion-based confocal smFRET to interrogate mGlu conformational changes at the appropriate (i.e. sub-ms) time resolution. We carefully evaluate the impact of different detergents on the functional integrity of solubilized receptor dimers. We demonstrate a compromised and inconstant response to orthosteric and allosteric ligands under previously reported detergent conditions, which is circumvented using an optimized detergent mixture composed of LMNG-CHS-GDN. Under these conditions the functional allosteric link between the orthosteric ligand binding site in the receptor's ECD and the site of allosteric modulation within the 7TM remains intact for significantly long time periods. This allowed us to study the impact of various classes of ligands on the conformational intersubunit rearrangement of the VFTs in full-length receptor dimers, using smFRET on freely diffusing single molecules. We show that the apo receptor samples an ensemble of conformations at the submillisecond timescale, and that full activation through reduction of these conformational dynamics requires the synergistic effect of an orthosteric and an allosteric modulator. This allosteric effect on VFT reorientation can be in differentially promoted by the synthetic positive allosteric modulator (PAM) BINA or purified heterotrimeric protein Gαi1Gβ1Gγ2 (G_i). In addition, our data demonstrate that a lack of full activation by partial agonists stems from their inability to stabilize the VFTs in their active state, that is partially, but not totally relieved by the addition of a PAM or G_i and remains related to agonist efficacy. Finally, we reveal that glutamate (Glu) alone, although classified as a full agonist, is unable to promote the full transition of mGluR2 VFTs to the active state, appearing to be less efficient than the compound LY37, and requiring a PAM to reach this fully stabilized state.

Results

Development of optimized detergent conditions for investigating mGlu2 receptor in micelles

Full-length mGlu2 receptors extracted from the cellular plasma membrane are required to be functional for several hours at room temperature, making the receptor solubilization our first challenge to overcome. We thus evaluated different detergents commonly used for GPCR-

solubilization including IGEPAL, n-Dodecyl β-D-maltoside (DDM), lauryl Maltose Neopentyl Glycol (LMNG) and glyco-diosgenin (GDN), supplemented or not with the cholesterol analogue cholesteryl hemisuccinate (CHS). The functional integrity of these mGlu2 dimers in detergent micelles was evaluated using lanthanide resonance energy transfer (LRET) measurements on N-terminally SNAP-labeled receptors(Selvin 2002; Doumazane et al. 2013; Scholler et al. 2017) after solubilization from crude HEK293T membrane fractions (Figure 2a). The dose-dependent FRET-decrease in response to Glu reported on the orthosteric activation of the receptor (i.e. the functionality of the ECD), whereas the integrity of the transmembrane domain was evaluated through the effect of the PAM BINA. Indeed, the PAM-binding site is known to be located within the 7TM region(O'Brien et al. 2018) and thus the functional link translating the PAM effect to Glu potency at the VFT level provides a reliable measure of the receptor's global functional integrity. In order to assess the receptor's functional integrity as a function of time in detergent micelles, measurements were repeated at various time points up to 24 hours of receptor storage at room temperature.

Most notably, receptors responded to Glu in a dose-dependent manner for all tested detergent conditions, as reflected by a decrease of the FRET signal as a result of VFT reorientation upon orthosteric activation (dose-response curves at time point 0 in Figure 2b-c, top (black) and S1-11). On the contrary, the response to PAM was strongly dependent on the detergent mixture used. No effect of positive allosteric modulation was observed using IGEPAL and DDM, two nonionic detergents that have previously been used to solubilize full-length mGluRs for smFRET by TIRF microscopy(Vafabakhsh, Levitz, and Isacoff 2015) (Figure 2b, top panel, compare black and blue curves; Figures S1 and S2). A very low effect of the PAM was observed when DDM was supplemented with CHS, a cholesterol analogue well-established to facilitate functional GPCR solubilization through mixed sterol-detergent micelles(Thompson et al. 2011). Nevertheless, this effect was lost within 4-6 hours and both pEC50 values for Glu and Glu+BINA decreased over time (Figure S3). Similarly, the branched nonionic detergent LMNG alone provided receptors with a more pronounced initial response to PAM but once again it rapidly decreased over time and was no longer

detectable after 24h (Figures 2c and S4). In contrast, a very positive dose-dependent effect on the functional integrity of receptors over time was observed by combining LMNG with increasing concentrations of CHS (Figures S5-7).

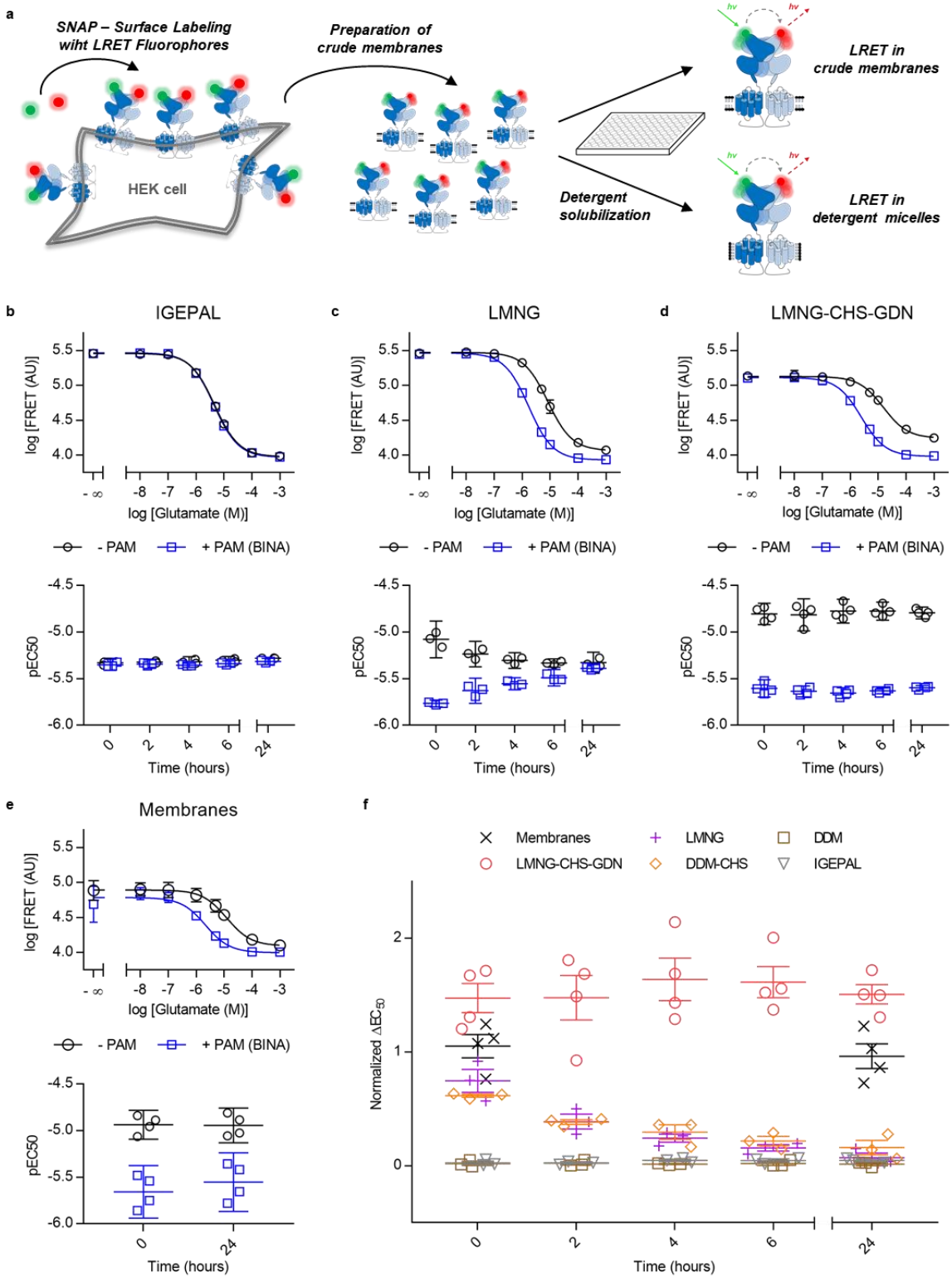

Figure 2:Evaluation of detergents for functional solubilization of full-length mGlu2 using LRET. a) SNAP-mGlu2 dimers were labeled with cell-impermeable lanthanide donor and green acceptor fluorophores on living HEK cells. After preparation of crude membrane fractions, LRET measurements were performed in microtiter plates either directly on

membranes or after detergent solubilization. b-f) The functional integrity of SNAP-labeled receptors was monitored over time at room temperature based on the dose-dependent intersubunit LRET changes in response to the orthosteric agonist Glu (- PAM) and in combination with 10µM positive allosteric modulator (+ PAM (BINA)). Solubilization with IGEPAL did not show any effect of BINA (b), receptors in LMNG micelles responded with an initial increase in Glu potency that was quickly lost over time (c). In contrast, a mixture of LMNG-CHS-GDN provided receptors with a strong and stable response up to at least 24h (d), with pEC50 values comparable to those obtained from mGluR2 in crude membranes (e). (f) Comparison of the potency difference between Glu and Glu+BINA (ΔEC_{50} normalized to crude membranes) for different detergents showed a stable effect of BINA in LMNG+CHS+GDN, an initial response in LMNG and DDM-CHS that was quickly lost over time and no effect in IGEPAL and DDM alone. Data represent the mean of triplicate analysis from 3-4 biological replicates. Errors are given as standard deviation of the mean in dose-response curves (b-e, top) and for ΔEC_{50} (f) and the 95% confidence interval of the mean for pEC50 values (b-e, bottom).

All tested CHS concentrations provided a pronounced initial PAM effect that lasted for 6 hours at a minimal CHS concentration (Figure S5) up to 24 hours at elevated concentrations (Figure S6-7).

The addition of GDN to the LMNG-CHS mixture further improved the time-dependent functional response of our receptor preparations. This steroid-based amphiphile has been demonstrated to improve GPCR functional integrity(Chae et al. 2012) and was recently employed in structure determination of mGluR5 by cryo-EM(Koehl et al. 2019). Although solubilized mGlu2 dimers maintained their functionality over time at all tested concentrations (Figure 2d and S8-10), the optimal reproducibility was found at a final concentration of 0.005% GDN (w/v). Interestingly, under these conditions, GDN and CHS concentrations remained moderate (0.005% w/v and 0.0004% w/v, respectively), which turned out to be advantageous for our smFRET studies as both chemicals were slightly contaminated with fluorescent species of unknown origin (also found in batches from different suppliers). Of note, in the absence of CHS, LMNG-GDN micelles provided a strong initial PAM effect, but a rapidly decreasing Glu pEC50 was observed, although the Glu+BINA pEC50 remained stable (Figure S11). Under these optimized conditions presented in Figure 2d, the observed FRET range as well as the pEC50 values of Glu and Glu+PAM were well in agreement with those obtained for mGlu2 dimers in crude membranes (Figure 2e and S12).

Overall, our detergent optimization demonstrated that a mixture of LMNG-CHS-GDN is superior to all other conditions tested. It allows maintaining full-length mGlu2 receptors in solution in a functional form, reflected by stable responses to orthosteric full and partial agonists as well as allosteric modulators over extented periods of time at room temperature (Figure 2d and f, S9, S13)

and in a similar manner as seen on mGlu2-containing crude membranes (Figure 2e and S12) and in live cells (Doumazane et al. 2013; Olofsson et al. 2014).

Agonists stabilize the active state with different efficacies

Having established the proper conditions for maintaining functional full-length mGlu2 freely diffusing in solution, we substituted the fluorophores used in LRET experiments with single molecule FRET compatible dyes (Figure 3a, Cy3B-BG-donor and d2-BG-acceptor(Olofsson et al. 2014)). We employed smFRET(Ha et al. 1996) with nanosecond ALEX(Laurence et al. 2005)/pulsed interleaved excitation (PIE)(Müller et al. 2005) and multiparameter fluorescence detection (MFD)(Kudryavtsev et al. 2012b), a technique that provides for each single molecule: i) its apparent FRET efficiency (E_{PR}), calculated from the spectral information, ii) its anisotropy (r), determined from the polarization of the photons, and iii) the average fluorescence lifetime of the donor dye in presence of the acceptor ($t_{D(A)}$). Thanks to the PIE experimental configuration, the average excited state lifetime of the acceptor dye (t_A) is verified as well, and only donor-acceptor (D-A) containing complexes are selected based on the stoichiometry factor S_{PR}(Hellenkamp et al. 2018).

The E_{PR} values obtained for full-length mGlu2 showed a wide, multimodal distribution (Figure 3b, left column black, Apo), indicating the co-existence of several conformational states. In the absence of ligands, a main population was centered around E_{PR}~0.6 (hereafter designated as the high FRET population, HF), and less well-defined minor populations were present at lower and high E_{PR} values. Qualitatively, this distribution reflected the one previously obtained by smFRET performed on isolated VFTs(Olofsson et al. 2014).

Upon application of saturating concentrations of the orthosteric partial agonists LCCG-I, DCG-IV or full agonist Glu a second major population at low FRET (LF) appeared, which was centered around E_{PR}~0.34 for all three ligands (Figure 3b, left column black). The fraction of molecules found in this LF population visibly increased with agonist efficacy, at saturating concentrations following LCCG-I<DCG-IV<Glu, and in a dose-dependent manner (see Figure 4b for Glu for example). The fraction in the HF population decreased accordingly, thus indicating a transition of molecules from HF to LF.

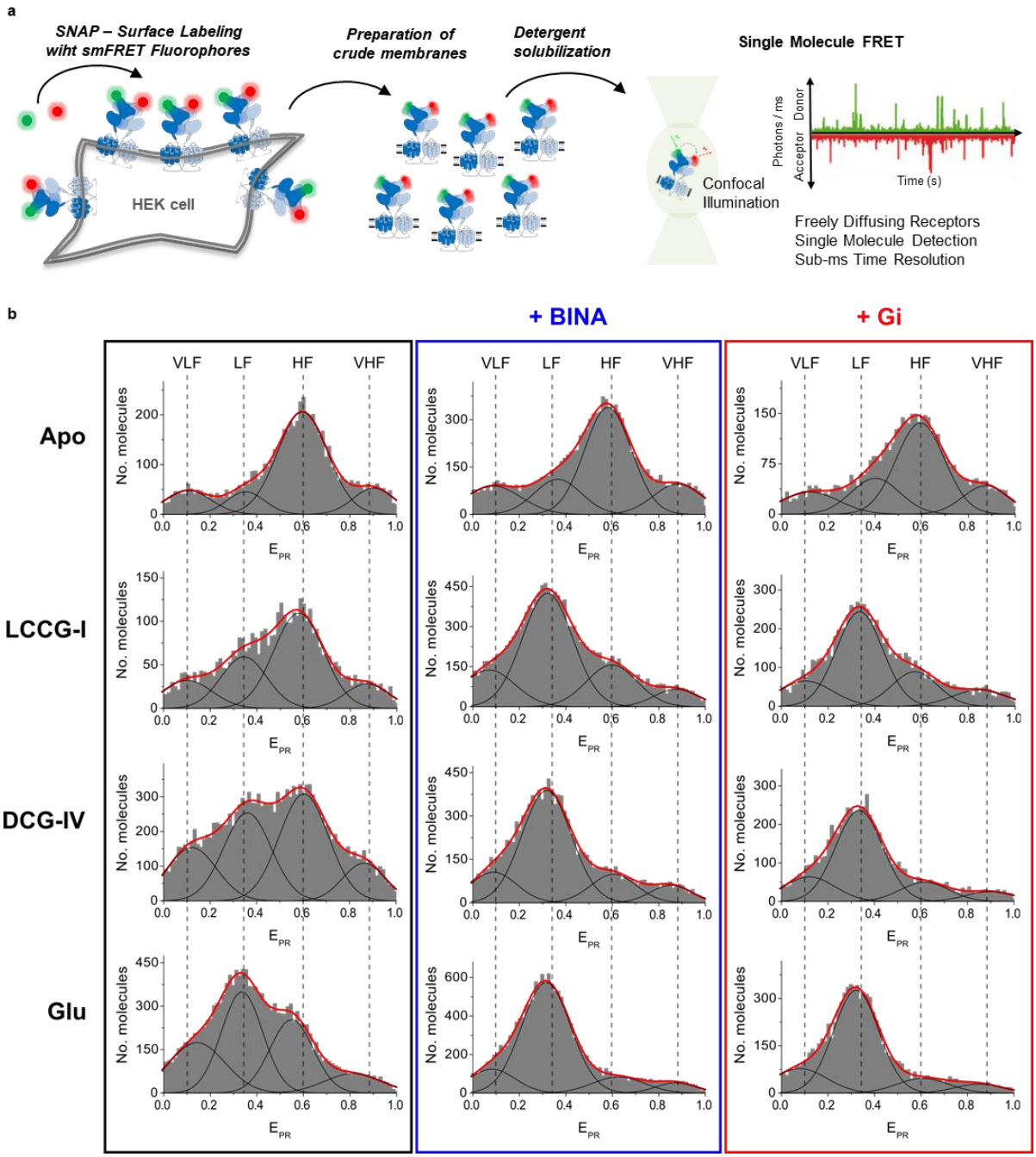

Figure 3: smFRET reveals the conformational landscape of full-length mGlu2 in LMNG-CHS-GDN micelles. a) SNAP-mGlu2 dimers were labeled with cell-impermeable Cy3b donor and D2 acceptor fluorophores on living HEK cells. After preparation of crude membrane fractions, mGlu2 dimers were detergent solubilized and smFRET measurements were performed on freely diffusing molecules with confocal illumination. b) Histograms display the number of detected, doubly labeled molecules as a function of apparent FRET efficiency (E_{PR}) between the N-termini of the VFT dimer. Rows: histograms in the absence (Apo) and presence of saturating concentrations of orthosteric agonists with increasing reported efficacy (LCCG-I<DCG-IV<Glu). Columns: histograms in the absence or presence of saturating PAM (+ BINA) or G protein (+ G_i). All histograms revealed 4 major populations denoted as very low FRET (VLF), low FRET (LF), high FRET (HF) and very high FRET (VHF). Black lines represent Gaussian fitting, red lines correspond to the cumulative fitting (see text).

This shift of the receptor population to a lower E_{PR} value was expected from our LRET measurements, smFRET observations on immobilized full-length receptors(Vafabakhsh, Levitz, and Isacoff 2015) and freely diffusing VFTs(Doumazane et al. 2013; Olofsson et al. 2014). We also noted that the

populations at very low FRET (E_{PR}~0.1, VLF) and very high FRET (E_{PR}~0.87; VHF) were present in all conditions, although their relative fractions were not subjected to important changes (Figure S14c and d).

From these observations, we concluded that the ensemble of populations at high FRET (HF+VHF) corresponds to an ensemble of conformations reflecting the resting/inactive state of the receptor, while the populations at low FRET (LF+VLF) can be attributed to receptors in the active state. Of note, no obvious basal activity of the apo receptor under these conditions was found, as saturating concentrations of the competitive orthosteric antagonist LY34 led to a similar distribution as the apo receptor (Figure S15a). This also rules out the presence of residual Glu in our receptor preparations, which was further verified by titration with LY34 in LRET measurements (Figure S13a-e, grey curves).

G protein or allosteric modulators in the 7TM are required to stabilize the mGlu2-VFT in the fully active state

Ensemble LRET measurements in live cells(Doumazane et al. 2013), crude membrane fractions (Figure 2e and S12) and detergent micelles (Figure 2d, S9 and S13) demonstrated that the VFT reorientation reports on the effect of allosteric modulation at the 7TM level by an increase in agonist potency and efficacy (Figure S16). Nevertheless, up to now the effect of allosteric modulators on the conformational landscape of the VFT in full-length mGlu2 receptors at the single molecule level remains unknown. We therefore applied BINA at saturating concentration, which led to a relative increase of the active population that was stronger than for each of the ligands alone (Figure 3b, compare center blue and left black columns). Consistent with the requirement of an agonist to be present for a pure PAM to exert its activity, no effect was observed in the absence of orthosteric ligands (Figure 3b, top row, Apo). We therefore concluded that BINA allosterically favors the stabilization of the mGlu2-VFT active state promoted by the orthosteric ligands.

In order to map the entire conformational landscape of the mGlu2-VFT we further analyzed the potential influence of the heterotrimeric G_i protein. Interestingly, addition of saturating concentrations of G_i led to nearly identical changes in the FRET distributions as promoted by PAM, both in presence and absence of ligand (Figure 3b, right red column). The combination of BINA and G_i did not lead to a further increase of the LF population (Figure S15b). Thus, PAM as well as G_i exert an allosteric effect through the 7TM, which is required to obtain a maximal shift of the VFT toward the active state. Most notably, under all described conditions, no additional populations or substantial changes in their peak position (E_{PR}) were found. This indicates that even if BINA and G_i promote an alternative conformation at the level of the 7TM, their allosteric effect on the VFT dimer conformation is explained by a simple shift of equilibrium toward the active state, rather than the stabilization of alternative states.

Comparison of orthosteric agonists reveals that glutamate has not the highest efficacy

The marked differences in the fractions of the FRET populations promoted by the different ligands (Figure 3b) prompted us to quantitatively analyze their fractional contributions. Therefore, we fitted all distributions with four gaussians at fixed E_{PR} and full width half maximum (FWHM) values obtained from the mean of all data sets (Figure S14a and b). This allowed us to determine the extent of VFT activation by calculating the fraction of receptors in the active state, i.e. the fraction of molecules found in the LF+VLF states relative to all molecules (Figure 4a).

By plotting this value as a function of Glu concentration, we obtained dose-response curves, which allowed us to determine pEC50 values in the absence or the presence of saturating concentrations of BINA (Figure 4b, black and blue curves, respectively). pEC50 values were in good agreement with those obtained from ensemble LRET on membranes (Figure 2e) or in detergent micelles (Figure 2d). The allosteric effect of BINA on the apparent Glu potency (an increase by almost one order of magnitude) as well as its effect on the maximum activation were also recovered, further validating the robustness of our solubilization strategy for mGlu2 to be employed in smFRET. This effect was also reversible, as adding a saturation concentration (10 µM) of the negative allosteric modulator

(NAM) ro64 decreased the fraction of active receptor obtained with 500nM BINA + Glu to the level observed in the presence of Glu alone (Figure 4c).

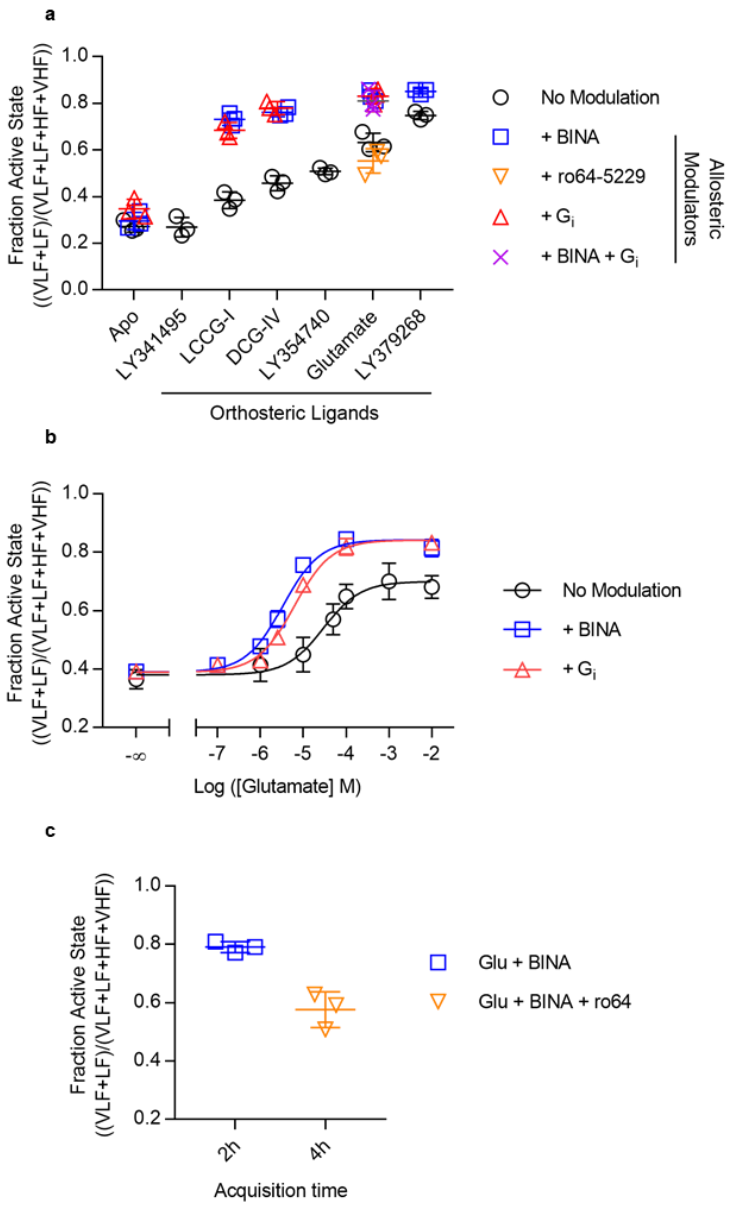

Figure 4: Fraction of active states in response to orthosteric and allosteric ligands. Fraction of active states is defined as the fraction of molecules found in the LF+VLF populations averaged over all molecules. a) Effect of different orthosteric and allosteric ligands on the fraction of molecules in the active state. BINA and G_i increase the fraction of molecules in this state, with an efficiency that depends on the ligand. In all cases, VFT reorientation is correlated with reported agonist efficacies (LCCG-I<DCG-IV<LY35<Glu<LY37). b) Glu dose-response curves in the absence (No modulation) and presence of PAM (+ BINA) or G_i obtained by smFRET reveal the increase of agonist potency and efficacy. c) Reversibility of the PAM-induced VFT activation by NAM was demonstrated by smFRET acquisition in the presence of 500nM BINA (2h) followed by addition of 10µM ro64 (4h). All scatter plots show the data from 3 independent biological replicates with mean and standard deviation.

Interestingly, Glu titration in the presence of saturating concentration of G_i (1µM) gave similar results as obtained with BINA (Figure 4b, red and blue curves, respectively). This demonstrates that G_i acts as an allosteric modulator on Glu potency and mGlu2 activation, although through distinct interaction sites in the 7TM other than BINA and thus most likely through distinct mechanisms. The efficacy of various agonists to promote the transition of the VFT toward the active state was quantified as well using this analysis (Figure 4a, black circles). In the absence of allosteric modulator, the fraction of mGlu in the active state increases at saturating concentration of each agonist, as follows : LCCG-I<DCG-IV<LY35<Glu<LY37 (Figure 4a). This is well in agreement with previous findings of VFT

reorientation obtained by LRET on live cells(Doumazane et al. 2013).

In addition, this analysis revealed that the agonist LY37 appears more potent than glutamate to push the receptor's VFT toward its active state. This observation points to the possibility that LY37 might qualify as a superagonist, i.e. a compound that displays greater efficacy and thus higher receptor signaling output, than the endogenous agonist glutamate(Schrage et al. 2016).

Representation of VFT activation in this way further revealed that the maximal effect is promoted by LY37+BINA. The individual effects of LCCG-I, DCG-IV and Glu in the presence of BINA or G_i were found to be lower, with an amplitude once again reflecting their efficacy. This observation reveals that these partial agonists are unable to fully stabilize the receptor VFT dimer in its active conformation, even in the presence of BINA or heterotrimeric G_i.

Our LRET data demonstrated that receptors only provide a strong and stable response to PAM in LMNG-CHS-GDN micelles, while in IGEPAL micelles this effect was completely absent (Figure 2, S1 and S10). To further understand the differential effects of the detergent mixture on full-length mGlu2 functionality, we analyzed the effect of Glu, BINA, G_i and ro64 on receptors solubilized with IGEPAL by smFRET (Figure S17). smFRET histograms allowed us to differentiate the major ligand induced effects relative to the apo receptor, despite the presence of elevated fluorescent contaminations. In contrast with the data obtained in LMNG-CHS-GDN, and in accordance with those obtained by LRET in IGEPAL (Figure 2b), we found a total shift of the molecules from the HF inactive to the LF active state induced by Glu, that was not further influenced by the addition of BINA or G_i.

In addition, the negative allosteric modulator ro64 showed a very modest effect on Glu potency in LMNG-CHS-GDN, well in accordance with results obtained by LRET in detergent and on membranes (Figure S9 and S12, respectively), while in IGEPAL no effect was observed at all (Figure S17). Overall our single molecule data in IGEPAL are well in agreement with the LRET data obtained in this detergent and in other suboptimal detergent mixtures (Figure 2). The observed loss of mGlu functionality in IGEPAL could arise from several phenomena: a loss of allosteric communication

between the 7TM and the ECD, a loss of structural integrity of the 7TM that becomes unable to bind the PAM or G protein, or a direct effect of IGEPAL on the conformation of the 7TM, stabilizing it in an active conformation that should only be reached in the presence of the allosteric modulator under proper conditions.

Stabilization of mGlu2 into the active state during activation

We then took advantage of the high time resolution of our measurements to uncover the hidden states, sampled by the receptor during its residence time in the confocal illumination volume, as we previously reported for the isolated ECDs (Olofsson et al. 2014)). Dynamic interconversion between several FRET efficiency states on the sub-diffusion timescale leads to averaging of the observed FRET efficiency, which depends on the observation time (~5 ms in our case).

Using two methods, we showed that most of the receptor dimers in the apo state are oscillating between the HF and the LF states at submillisecond timescales. First, when the donor fluorescence lifetimes τ_{DA} for each single molecule are plotted against the γ-corrected FRET efficiency *E* ("τ_{DA} vs. *E*" analysis (Sisamakis et al. 2010)), the main population of receptors in the apo state (at *E*~0.6) appeared above the static FRET line that represent a molecule exhibiting constant FRET during its residence time (Figure 5a). This indicated submillisecond conformational dynamics of the mGlu2 receptor. Second, these dynamics were confirmed by time windows analysis (TWA) (Gopich and Szabo 2010). We recalculated the FRET efficiencies from data originating from the doubly labeled molecules, using different integration times from 200 µs to 1 ms. The distribution obtained by integrating over 1 ms (Figure 5b, left, green) matched the one obtained from burst-integrated calculations (Figure 3, Apo), with a main population at *E*~0.6, indicating that there are no dynamics between 1ms and the residence time (~5 ms). However, shortening the integration time strikingly led to the disappearance of this HF population, while two populations at *E*~0.2 and >0.9 were revealed (Figure 5b, left, yellow, red and blue). These changes in the distribution point to the fact that at submillisecond timescales, the apo receptor samples a set of conformations at low and very high *E*

values (Figure 5g). The apparent *E* at ~0.6 represents the time-averaged value between these two sampled states.

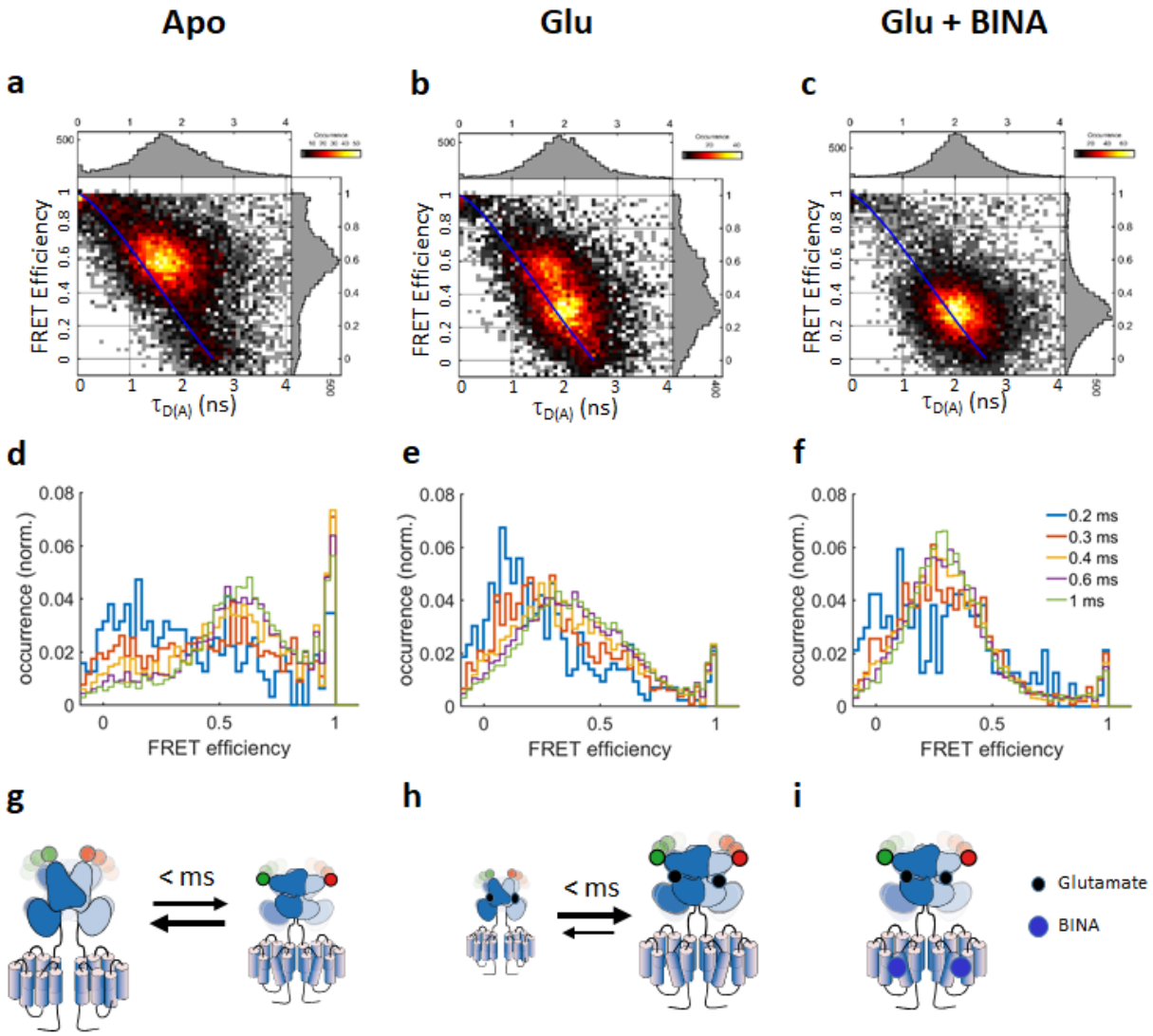

Figure 5: Structural dynamics analysis of mGlu2 dimers in response to orthosteric and allosteric ligands. a-c) Representative t_{DA} vs. E histogram for mGlu2 dimers in the absence (a, Apo) or presence of Glu (b) or Glu + BINA (c). For the Apo receptors, the major population deviates from the "Static FRET" line (blue), indicating conformational dynamics at the sub-millisecond time scale. Addition of Glu stabilizes the receptor VFT dimer in an ensemble of low FRET conformations with less flexibility, an effect that is reinforced by the allosteric modulator BINA. d-f) Time windows analysis for different integration times (from 0.2 to 1ms) reveals a large conformational flexibility of the Apo receptor VFT at 200-600µs timescales, that is strongly restricted when bound to orthosteric agonist and allosteric modulator. g-i) Schematic representation of the major species observed in all 3 cases, with the timescales of the transition between them. Black and blue dots represent Glu and BINA respectively. The size of the cartoon schematically represents the fraction of the species.

In contrast, addition of orthosteric and allosteric ligands promoted stabilization of the receptor in an ensemble of low FRET conformations, characteristic of the active states. The low FRET population that increases upon addition of these ligands is located just above (Glu, Figure 5c) or on the static FRET lines (Glu+BINA, Figure 5e), indicating that these molecules remain in a low FRET state

during their transit time. Similarly, in the TWA approach, some residual conformational dynamics are observed at the ~200 µs timescale. These are limited to conformations within the low FRET states, corresponding to "active" states of the receptor. Transitions to the inactive, high FRET states are considerably reduced in the presence of Glu alone (Figure 5d,h), and virtually eliminated when BINA is added (Figure 5f,i).

Analysis of "τDA vs. *E*" and TWA analyses for other ligands confirmed these observations (Figures S18-19). First, a fast conformational exchange between high FRET and low FRET states was observed with the orthosteric antagonist LY34, similarly to what was observed for the apo receptor. Second, this conformational heterogeneity was reduced in the presence of partial agonists, with an extent that correlated with their relative efficacies. Third, the "superagonist" LY37 was even more efficient than Glu to stabilize the receptors in the ensemble of active conformations. Fourth, "τ_{DA} vs. E" and TWA data obtained in the presence of G_i matched those obtained in the presence of BINA, confirming the ability of G_i to allosterically lock the VFTs in its active state. Finally, it should be noted that the TWA analysis of receptors solubilized in IGEPAL did not show conformational dynamics in the 200µs-1ms timescale, for both the apo and the Glu-bound receptors. This observation points to a loss of mGlu functional dynamic behavior in this detergent, correlated with the loss of allosteric modulation by BINA.

Discussion

Different classes of ligands acting either via orthosteric or allosteric sites are known to exert differential effects on GPCR activation. In mGlus, the orthosteric site is located in the VFT, while the vast majority of allosteric ligands interact with the 7TM (Figure 1). Pharmacologically, full agonists are characterized by exerting a maximal cellular response, whereas partial agonist-induced responses are submaximal. Such measures of receptor activation typically rely on downstream second messenger accumulation, gene regulation or transducer activation. However, orthosteric ligand action has been directly related to the extent of VFT reorientation on N-terminally-labeled mGlu dimers,

probed by LRET on live cells(Doumazane et al. 2013; Scholler et al. 2017). In addition, this N-terminal intersubunit sensor also reports on the effect of allosteric ligands in full-length receptors, thereby reflecting the allosteric communication between VFT and 7TM. This allowed to demonstrate that PAMs can facilitate maximal efficacy of orthosteric activation by partial agonists. These observations indicate the important role of a well-balanced dynamic conformational equilibrium of the VFT between different preexisting states that is allosterically connected to the dimeric transmembrane domain, to achieve a fine-tuned regulation of receptor activation.

smFRET is perfectly suited to explore such conformational changes in real time. Previous studies have so far been limited to the exploration of orthosteric modulation, in the context of isolated VFTs(Olofsson et al. 2014), or on immobilized full length homo-(Vafabakhsh, Levitz, and Isacoff 2015) and heterodimers(Levitz et al. 2016; Habrian et al. 2019). Here, we report the effect of various allosteric modulators on the mGlu2 conformational landscape, on isolated, fully functional, full-length receptors and with submillisecond time resolution.

Through a careful optimization of solubilization conditions, we demonstrate that the functional integrity of full-length mGlu2 can be maintained for hours at room temperature (Figure 2d and S9). This was only achieved using a mixture of LMNG-CHS-GDN, while all other tested conditions employing popular detergents such as IGEPAL and DDM but also DDM-CHS, LMNG-CHS and LMNG-GDN exhibited a time-dependent impact on receptor function as judged by changes in the apparent pEC50 values obtained from VFT reorientation by LRET (Figure 2b-c and S1-7, 11). It is not surprising that a functional reconstitution of multidomain, multimeric membrane proteins such as mGlu require adapted characteristics to account for proper folding, ligands binding and activity. The combination of MNG and CHS was shown to be required for a proper activation of purified mGlu5 to the G_q protein(Nasrallah et al. 2018). Improved GPCR functionality by the branched nonionic detergent LMNG has been described to result from an enhanced stabilization of the 7TM due to a lower detergent exchange rate as compared to its single aliphatic counterpart DDM, thereby confining receptor motions in a way similar to lipids(S. Lee et al. 2020). In addition, enhanced polar interactions

of the maltosid head of LMNG with loops and 7TM ends may play an important role in maintaining the functional link between the VFT and the 7TM through the CRD, e.g. by stabilizing the extracellular loop 2 known to be essential for this coupling (Koehl et al. 2019). Further stabilization and function promoting properties are provided by the two sterol-containing compounds CHS and GDN. CHS is structurally very similar to cholesterol and has been observed in the extra-helical parts of TM1 and TM2 of the mGlu1 7TM structure 4OR2(Wu et al. 2014). Furthermore, cholesterol was found to act as an allosteric modulator on the CRD of the smoothened receptor(Huang et al. 2016). In contrast to LMNG and GDN, CHS further provides a net negative charge to the detergent micelles, which might exert a positive effect on allosteric modulator action. Negative charges have been described to enhance agonist affinity and stabilize the active state of the β2-AR(Strohman et al. 2019), a prototypical class A GPCR, whose orthosteric binding site comprises similar features to that of the allosteric site in mGlu(Feng et al. 2015). Finally, GDN is characterized by a dimaltose head group and a sterol-based tail thus combining similar features to the LMNG head and CHS. Nevertheless, the triple combination LMNG-GDN-CHS was required to stabilize receptor function over time, pointing to a complementary role of GDN providing additional glycol head groups and sterol moieties without bringing negative charges as CHS.

LRET measurements in this improved mixture clearly revealed that the PAM was required to reach the maximum efficacy in terms of VFT reorientation toward the active states. Indeed, this effect was only partial with Glu alone, as also observed on crude membrane fractions although to a lower extent (Figure S16).

Establishing the proper conditions for mGlu2 functional stabilization at room temperature allowed us to perform single molecule FRET measurements on diffusing molecules for several hours. This was required to obtain data with a good statistical sampling of all states populated by the receptor, followed by analysis of its structural dynamics. It revealed the presence of 4 VFT states, of which two - the HF/inactive and LF/active states - are predominantly populated, in a ligand-dependent manner (Figure 3b and S15). Similar to our observations on isolated ECD dimers(Olofsson et al.

2014), we observed the presence of a very high FRET and a very low FRET conformation, but could not detect whether these population were in exchange with the other ones at timescales longer than our observation time (> 5ms). The effect of ligands on the population of these minor states, if any, was minimal (Figure S14c-d). However, the conformational landscapes of the most populated receptor population differed from the one observed for the isolated VFT dimers. In that latter case, all dimers were shown to be oscillating at a ~100µs timescale between the high and low FRET states. All ligands tested simply pushed this equilibrium towards one of the states, but the fast conformational dynamics were always retained. Here, in the case of full-length receptor dimers in the apo state or bound to antagonist, the main population is similarly oscillating between the HF and LF states (at a slightly slower, 200-500µs timescale). But in contrast to the isolated VFT, addition of the full agonist led to a stabilization of an ensemble of LF conformations that appear stable for several milliseconds, a duration compatible with the activation of downstream signaling(Marcaggi et al. 2009; Grushevskyi et al. 2019). We propose that this stabilization of the active conformation of the full-length receptor stems from a strengthening of the dimeric interface, probably via interactions involving transmembrane helix 6 (TM6) in the active state. This strengthening has been proposed, by comparing the cryo-EM structures of the apo mGlu5 in nanodiscs, and the active mGlu5 in GDN micelles, bound to an agonist, a PAM, and a stabilizing nanobody(Koehl et al. 2019). Evidence of a transition from a TM4/TM5 dimeric interface to a TM6 interface upon PAM-driven activation also came from crosslinking experiments on mGlu2(Xue et al. 2015) and well as on the related class C GPCR $GABA_B$ (Xue et al. 2019). And finally, an effect of PAMs on the dimeric interface of several truncated 7TM dimers was demonstrated using an ensemble FRET sensor(Gutzeit et al. 2019). Here, we show on full-length receptors that a stabilization of the active state indeed occurs upon agonist binding, that it lasts for at least several milliseconds, and that it is reinforced by the presence of the transmembrane domain, through allosteric interaction with G_i protein or positive allosteric modulator. It is interesting to note that the full stabilization of the active state is not achieved even at saturation of the natural agonist Glu. In contrast, LY37, formally considered as a full agonist, appears in our

assay more efficient than Glu in promoting the adoption of the VFT's active state, which qualifies this molecule as a "superagonist"(Schrage et al. 2016). This effect is likely not observed in classical cell-based, pharmacological assays, where the G protein, acting as allosteric modulator to promote the active state, is always present. Indeed, in our smFRET assay, the distribution of states obtained upon activation in the presence of PAM was identical for receptors bound to Glu and LY37, reflecting the conditions of the cell-based assays were a difference in efficiency between these molecules cannot be detected.

Finally, our data demonstrate that the effect of all the tested partial agonists stems from a lack of their ability to stabilize the active conformation of the receptor dimers, as we inferred from our previous smFRET study on isolated VFTs(Olofsson et al. 2014). Indeed, we still do not observe new additional populations with an intermediate FRET efficiency upon binding of these molecules. Instead, we are able to demonstrate a reduction of the receptor's structural dynamics and a population of the active states, that correlates with the efficacy of these agonists. A model, where these partial agonists stabilize alternative receptor conformations that are not fully potent in activating downstream signaling can therefore be excluded. We also note that, in the presence of partial agonists, addition of a PAM or G_i was not sufficient to promote the stabilization of the active state to the extent observed with Glu and LY37. This observation is perfectly consistent with the fact that these molecules were qualified as partial agonists for mGlu2 activation in cell-based pharmacological assays where the G protein is generally present.

Overall, the strategy proposed here to stabilize functional and soluble mGlu2 dimers paves the way for future experiments that aim at dissecting with high spatial and temporal resolution the relative and coordinated movements of all domains of the mGlu dimers. This could be achieved after incorporation of non-canonical amino acids at strategic residues, followed by fluorescent labeling and high-precision smFRET measurements(Tian, Furstenberg, and Huber 2017). This will evidently pave the way for a deeper understanding of how mGluR dynamics regulate their function and may open up new routes for the development of fine-tuned therapeutics.

Acknowledgements

We thank : Sebastien Granier and Remy Sounier (IGF Montpellier, France) for providing the heterotrimeric G protein ; Gilles Labesse (CBS Montpellier) for helping in mglu2 modelling ; Suren Felekyan (U. Dusseldorf, Germany) for discussion on data analysis ; Guillaume Lebon (IGF Montpellier, France) and the members of the IBM team (CBS Montpellier) for fruitful discussions. Our research is supported by grants from the Agence Nationale pour la Recherche (ANR 17-CE09-0026-02 to EM & ANR 18-CE11-0004-02 to EM & JPP), and the Fondation Recherche Médicale (DEQ20170336747 to JPP). AMC was supported by the Labex EPIGENMED The CBS belongs to the France-BioImaging national infrastructure supported by the French National Research Agency (ANR-10-INBS-04, “Investments for the future”) and is supported by the GIS "IBiSA: Infrastructures en Biologie Sante et Agronomie".

Competing Financial Interest Statement

The authors declare no competing financial interest.

Materials and Methods

Chemicals

All chemicals were purchased from Sigma-Aldrich, Merck and Roth unless otherwise noted. n-dodecyl-β-D-maltopyranoside (DDM), lauryl maltose neopentyl glycol (LMNG) and cholesteryl hemisuccinate (CHS) tris salt were purchased from Anatrace (through CliniSciences, France). Glyco-diosgenin (GDN) was purchased from Avanti Polar Lipids through Merck. SNAP-Lumi4-Tb, SNAP-green, SNAP-Cy3b and SNAP-D2 were obtained from Cisbio Bioassays (Codolet, France). DCG-IV, LY341495, LY379268, LY354740, LCCG-I, BINA hydrochloride and Ro64-5229 were purchased from Tocris Bioscience (Bristol, UK).

Plasmids

The pcDNA plasmid encoding SNAP-tagged human mGluR2 was a gift from Cisbio Bioassays (Codolet, France).

Cell culture

Adherent HEK293T cells (ATCC CRL-3216, LGC Standards S.a.r.l., France) were cultured in Gibco™ DMEM, high glucose, GlutaMAX™ Supplement, pyruvate (Thermo Fisher Scientific, France) supplemented with 10% (vol/vol) FBS (Sigma-Aldrich, France) at 37°C, 5% CO_2 and passaged twice per week.

Transfection and Labeling

$1x10^7$ cells were seeded in 75cm^2 flasks 24h prior to transfection with Polyethylenimine (PEI 25K, Polysciences Europe GmbH, Germany) at a DNA to PEI ratio (w/w) of 3:1 using 12µg mGluR2 plasmid DNA per flask. In brief, 10mg/ml PEI stock solution in 1M HCl was diluted in 20 mM MES at pH5 with 150 mM NaCl and incubated at room temperature for 25min before sequential addition of 5 ml complete medium followed an additional 5 ml. The flask's culture medium was then replaced by the diluted transfection mix and protein expression proceeded for 48h at 37°C, 5% CO_2.

SNAP-tag labeling was performed on surface-adhered cells in DMEM GlutaMax without FBS for 1-2h at 37°C using final concentrations of either 100nM SNAP-Lumi4-Tb and 60nM SNAP-green for LRET or 600nM SNAP-Cy3b and 300nM SNAP-D2 for smFRET measurements. Following labeling, excess dye was removed by three cycles of washing with DPBS w/o Ca^{2+} and Mg^{2+} (Thermo Fischer Scientific, France) at ambient temperature.

Preparation of crude membrane fractions

Adherent cells were detached mechanically using a cell scraper in DPBS w/o Ca^{2+} and Mg^{2+} (Thermo Fisher Scientific, France) and collected at 500xg and 22°C. Subsequently, cells were resuspended in cold hypotonic lysis buffer (10mM HEPES pH7.4, cOmplete™ protease inhibitor), frozen and stored

at -80°C. After thawing, cells were passed through a 0.4mm gauge needle 30-times using syringe on ice. After two rounds of centrifugation at 500xg and 4°C for 5min, the supernatant was aliquoted and centrifuged at 21,000xg and 4°C for 30min to collect crude membranes. The pellets were washed once with 20mM HEPES pH7.4, 118mM NaCl, flash frozen in liquid N_2 and stored at -80°C.

Detergent solubilization

Receptors were solubilized on ice by resuspension of crude membranes in acquisition buffer (20mM Tris-HCl pH7.4, 118mM NaCl, 1.2mM KH_2PO_4, 1.2mM $MgSO_4$, 4.7mM KCl, 1.8mM $CaCl_2$) supplemented with 1% (v/v) IGEPAL, 1% (w/v) DDM, 1% (w/v) DDM + 0.2% (w/v) CHS tris, 0.1% (w/v) LMNG, 0.1% (w/v) LMNG + 0.1% GDN (w/v), 0.1% (w/v) LMNG + 0.004%, 0.008% or 0.016% CHS tris (w/v) or 0.1% (w/v) LMNG + 0.008% (w/v) CHS tris + 0.05%, 0.1% or 0.2% GDN (w/v). After 5min, the solution was centrifuged for 10min at 21,000xg and 4°C. The supernatant was then applied to a Zeba Spin Desalting Column (7 kDa cut-off, Thermo Fisher Scientific, France) equilibrated in acquisition buffer containing 5% of the detergent concentration used for solubilization and centrifuged 2min at 1,500xg and 4°C. The flow-through was then immediately diluted 1:20 in cold acquisition buffer and kept on ice in the dark until use.

LRET

Intersubunit LRET measurements of mGluR2 dimers, N-terminally labeled with the Lumi4-Tb donor and the green acceptor via an engineered SNAP-tag, were performed on a PHERAstar FS microplate reader (BMG Labtech, Germany) in white 384 well plates (polystyrene, flat-bottom, small volume, medium-binding, Greiner Bio-One SAS, France). Measurements where performed in acquisition buffer in the presence of indicated ligands at room temperature and plates where sealed and stored in the dark in between measurements for time course experiments to minimize evaporation and fluorophore bleaching. The fluorescence decay of donor and acceptor was recoded using the LRET 337/620/520 optical module by excitation with 20 flashes per well every 5µs for a total of 2500µs. The FRET signal was expressed as sensitized acceptor emission integrated between 50-100µs and

normalized to its emission between 1200-1600µs as previously optimized for the given mGluR2 FRET sensor (Scholler et al. 2017).

Expression and purification of heterotrimeric G_{i1}

The heterotrimeric Gi1 complex was a kind gift from Sebastien Granier and Remy Sounier (IGF Montpellier, France). G_{i1} heterotrimer was expressed in *Sf*9 insect cells in EX-CELL 420 media (Sigma). Human $G_{\alpha i1}$ was cloned into the pVL1392 vector, and the virus was prepared using the BestBac system (Expression System, LLC). N-terminal Flag-tagged human $G_{\beta 1}$, and human $G_{\gamma 2}$ were cloned into the pFastBac vector, and the virus was prepared using the Bac-to-Bac baculovirus system. The cells were infected with both $G_{\alpha i1}$ and $G_{\beta\gamma}$ virus at a ratio determined by small-scale titration experiments at 27°C for 48h before collection. Cells containing G_{i1} heterotrimer were lysed in hypotonic buffer containing 10 mM Tris pH7.4, 100 mM $MgCl_2$, 10 mM GDP, 5 mM β-mercaptoethanol, and protease inhibitors. After centrifugation, membranes were dounced and solubilized in buffer containing 20 mM HEPES pH7.5, 100 mM NaCl, 1% DDM, 5 mM $MgCl_2$, 10 mM GDP, 5 mM β-mercaptoethanol and protease inhibitors. Solution containing the G_{i1} heterotrimeric complex was loaded onto an anti-FLAG M1 affinity column. After washing of the column with 5 column volumes of buffer E1 (20 mM HEPES pH 7.5, 100 mM NaCl, 1% DDM, 5 mM $MgCl_2$, 10 mM GDP, 5 mM β-mercaptoethanol) and buffer E2 (20 mM HEPES pH 7.5, 50 mM NaCl, 0.1% DDM, 1 mM MgCl2, 10 mM GDP, 100µM TCEP) at a flow rate of 2 ml.min-1. After a detergent exchange was performed by washing the column with a series of seven buffers (3 CV each) made up of the following ratios (v/v) of MNG buffer (20 mM HEPES pH 7.5, 50 mM NaCl, 0.5% MNG, 1 mM MgCl2, 10 mM GDP, 100µM TCEP) and E2 buffer: 0:1, 1:1, 4:1, 9:1, 19:1, 99:1 and MNG buffer alone. Gi1 heterotrimer was eluted with Elution buffer (20 mM HEPES pH 7.5, 50 mM NaCl, 0.01% MNG, 1 mM MgCl2, 10 mM GDP, 100 µM TCEP). Eluted sample was concentrated in a 50 kDa MWCO concentrator to 100 µM and aliquots were flash frozen in liquid Nitrogen and stored at -80°C.

PIE-MFD smFRET setup

Single-molecule FRET experiments with pulsed interleaved excitation (PIE) – multiparameter fluorescence detection (MFD) were performed on a homebuilt confocal microscope as described previously(Olofsson and Margeat 2013).

In brief, the 20MHz-pulsed white excitation laser was split into two beams spectrally filtered using excitation bandpass filters at wavelength 532/10 (prompt beam) and 635/10 (delayed beam) to excite the Cy3b donor and D2 acceptor molecules, respectively. The delayed beam has a path length of ~ 8m relative to the prompt beam, generating a ~24ns delay in the pulse. The two beam paths are then recombined and focused using a 10x objective into a single-mode fiber, by which the beams become spatially overlapped and filtered. The output of the fiber is collimated using a 10x microscope objective lens, polarized and coupled into an inverted microscope (Eclipse Ti, Nikon, France). The excitation power was controlled to give 25 µW for the prompt and 12 µW for the delayed beam at the entrance into the microscope. Inside the microscope, the light is reflected by a dichroic mirror that matches the excitation/emission wavelengths (FF545/650-Di01, Semrock, Rochester, NY, USA) and coupled into a 100x, NA1.4 objective (Nikon, France). Emitted photons are then collected by the objective and focused on a pinhole of 150µm. The emission photon stream is collimated and divided using a polarizing beamsplitter. In each created polarization channel, the photons are spectrally separated using dichroic mirrors (BS 649, Semrock, Rochester, NY, USA) and filtered using high quality emission filters (parallel: ET BP 585/65, Chroma, Bellows Falls, VT, USA and FF01-698/70-25, Semrock, Rochester, NY, USA, perpendicular: HQ 590/75 M, Chroma, Bellows Falls, VT, USA and FF01-698/70-25, Semrock, Rochester, NY, USA). Single photons are detected using Single Photon Avalanche Diodes. We use two MPD-1CTC (MPD, Bolzano, Italy) for the donor wavelength channels and two SPCM AQR-14 (Perkin Elmer, Fremont, CA, USA) for the acceptor wavelength channels. The output of the detectors is coupled into a TCSPC counting board (SPC-150, Becker&Hickl, Berlin, Germany), through a HRT41 router (B&H), using appropriate pulse inverters and attenuators. The sync signal that triggers the TCSPC board is provided by picking a small fraction

of the light from the prompt path (reflected by a coverslip), and focusing it on an avalanche diode (APM-400, B&H).

smFRET measurements

Measurements were performed at concentrations of 30-100 pM on SensoPlate 384 well plates (non-treated, Greiner Bio-One, France) passivated with 10mg/ml bovine serum albumin (BSA) in acquisition buffer with detergent for at least 1h prior to sample application. Samples were measured in acquisition buffer with detergent and ligand concentrations as indicated in the text. Measurements at saturating ligand concentration were carried out at 10mM Glutamate, 100µM LY37, 100µM LY34, 1mM LCCG-I, 1mM DCG-IV and 1mM LY35. Allosteric modulators BINA and ro64 were supplemented at a final concentration of 10µM. The effect of BINA at 500nM was reversed by the addition of 10µM ro64. To study the effect of heterotrimeric human Gαi1Gβ1Gγ2 on VFT reorientation 1µM of the heterotrimer in the absence or presence of ligand was incubated with receptor (at approximately 30-100pM) for 30min at room temperature in the presence of 1µM TCEP, 100nM GDP, followed by the addition of 0.05U/µl of apyrase (Sigma-Aldrich, France) and incubation for another 30min before acquisition.

smFRET data analysis

Data analysis was performed using the Software Package for Multiparameter Fluorescence Spectroscopy, Full Correlation and Multiparameter Fluorescence Imaging developed in C.A.M. Seidel's lab (http:// www.mpc.uni-duesseldorf.de/seidel/) as described previously(Olofsson et al. 2014). A single-molecule event was defined as a burst containing of at least 40 photons with a maximum allowed interphoton time of 0.3 ms and a Lee-filter of 20. Photobleaching events were identified base on |TGX-TRR|<1 ms as described(Kudryavtsev et al. 2012a).

τ_{DA} vs E analysis and time windows analysis were performed using the PAM software(Schrimpf et al. 2018). The static FRET line for the τ_{DA} vs E analysis was plotted taking into consideration the excited state lifetime of the donor, and a 6Å dye linker length.

Apparent FRET efficiencies (EPR), FRET efficiencies (E) and Stoichiometry were calculated using the conventions and recommendations made in (N. K. Lee et al. 2005) and (Hellenkamp et al. 2018) Precision, i.e.

$$E_{PR} = {}^{iii}E_{app} = \frac{F_{A/D}}{F_{A/D} + {}^{ii}F_{Dem/Dex}}$$

$$E = \frac{F_{A/D}}{F_{A/D} + \gamma . {}^{ii}F_{Dem/Dex}}$$

Where,

${}^{ii}F_{Xem/Yex}$ is the background corrected intensity in the X emission channel upon Y excitation. $F_{A/D}$ are the detected intensities in the acceptor emission channel upon donor excitation, corrected for background, donor leakage α (fraction of the donor emission into the acceptor detection channel) and direct excitation δ (fraction of the direct excitation of the acceptor by the donor-excitation laser)

γ is the normalization factor that considers effective fluorescence quantum yields and detection efficiencies of the acceptor and donor.

Additional Software

LRET data was analyzed using the MARS (BMG Labtech) and displayed in GraphPad PRISM 7.05. FRET histograms were fitted and displayed using Origin 6 (Microcal Software, Inc.).

References

Chae, Pil Seok, Søren G. F. Rasmussen, Rohini R. Rana, Kamil Gotfryd, Andrew C. Kruse, Aashish Manglik, Kyung Ho Cho, et al. 2012. "A New Class of Amphiphiles Bearing Rigid Hydrophobic Groups for Solubilization and Stabilization of Membrane Proteins." *Chemistry - A European Journal* 18 (31): 9485–90. https://doi.org/10.1002/chem.201200069.

Doumazane, Etienne, Pauline Scholler, Ludovic Fabre, Jurriaan M Zwier, Eric Trinquet, Jean-Philippe Pin, and Philippe Rondard. 2013. "Illuminating the Activation Mechanisms and Allosteric Properties of Metabotropic Glutamate Receptors." *Proceedings of the National*

Academy of Sciences of the United States of America 110 (15): E1416-25. https://doi.org/10.1073/pnas.1215615110.

Feng, Zhiwei, Shifan Ma, Guanxing Hu, and Xiang Qun Xie. 2015. "Allosteric Binding Site and Activation Mechanism of Class C G-Protein Coupled Receptors: Metabotropic Glutamate Receptor Family." *AAPS Journal* 17 (3): 737–53. https://doi.org/10.1208/s12248-015-9742-8.

García-Nafría, Javier, and Christopher G. Tate. 2019. "Cryo-EM Structures of GPCRs Coupled to G s , G i and G O." *Molecular and Cellular Endocrinology*. Elsevier Ireland Ltd. https://doi.org/10.1016/j.mce.2019.02.006.

Gopich, Irina V, and Attila Szabo. 2010. "FRET Efficiency Distributions of Multistate Single Molecules." *The Journal of Physical Chemistry. B* 114 (46): 15221–26. https://doi.org/10.1021/jp105359z.

Grushevskyi, Eugene O., Taulant Kukaj, Ralf Schmauder, Andreas Bock, Ulrike Zabel, Tina Schwabe, Klaus Benndorf, and Martin J. Lohse. 2019. "Stepwise Activation of a Class C GPCR Begins with Millisecond Dimer Rearrangement." *Proceedings of the National Academy of Sciences*, April, 201900261. https://doi.org/10.1073/pnas.1900261116.

Gutzeit, Vanessa A, Jordana Thibado, Daniel Starer Stor, Zhou Zhou, Scott C Blanchard, Olaf S Andersen, and Joshua Levitz. 2019. "Conformational Dynamics between Transmembrane Domains and Allosteric Modulation of a Metabotropic Glutamate Receptor." *ELife* 8 (June). https://doi.org/10.7554/eLife.45116.

Ha, T, T Enderle, D F Ogletree, D S Chemla, P R Selvin, and S Weiss. 1996. "Probing the Interaction between Two Single Molecules: Fluorescence Resonance Energy Transfer between a Single Donor and a Single Acceptor." *Proc Natl Acad Sci U S A* 93 (13): 6264–68.

Habrian, Chris H., Joshua Levitz, Vojtech Vyklicky, Zhu Fu, Adam Hoagland, Isabelle McCort-Tranchepain, Francine Acher, and Ehud Y. Isacoff. 2019. "Conformational Pathway Provides Unique Sensitivity to a Synaptic MGluR." *Nature Communications 2019 10:1* 10 (1): 1–13. https://doi.org/10.1038/s41467-019-13407-8.

Hellenkamp, Björn, Sonja Schmid, Olga Doroshenko, Oleg Opanasyuk, Ralf Kühnemuth, Soheila Rezaei Adariani, Benjamin Ambrose, et al. 2018. "Precision and Accuracy of Single-Molecule FRET Measurements—a Multi-Laboratory Benchmark Study." *Nature Methods* 15 (9): 669–76. https://doi.org/10.1038/s41592-018-0085-0.

Hilger, Daniel, Matthieu Masureel, and Brian K. Kobilka. 2018. "Structure and Dynamics of GPCR Signaling Complexes." *Nature Structural and Molecular Biology* 25 (1): 4–12. https://doi.org/10.1038/s41594-017-0011-7.

Hlavackova, V., U. Zabel, D. Frankova, J. Batz, C. Hoffmann, L. Prezeau, J.-P. Pin, J. Blahos, and M. J. Lohse. 2012. "Sequential Inter- and Intrasubunit Rearrangements During Activation of Dimeric Metabotropic Glutamate Receptor 1." *Science Signaling* 5 (237): ra59–ra59. https://doi.org/10.1126/scisignal.2002720.

Huang, Pengxiang, Daniel Nedelcu, Miyako Watanabe, Cindy Jao, Youngchang Kim, Jing Liu, and Adrian Salic. 2016. "Cellular Cholesterol Directly Activates Smoothened in Hedgehog Signaling." *Cell* 166 (5): 1176-1187.e14. https://doi.org/10.1016/j.cell.2016.08.003.

Koehl, Antoine, Hongli Hu, Dan Feng, Bingfa Sun, Yan Zhang, Michael J. Robertson, Matthew Chu, et al. 2019. "Structural Insights into the Activation of Metabotropic Glutamate Receptors." *Nature* 566 (7742): 79–84. https://doi.org/10.1038/s41586-019-0881-4.

Kudryavtsev, Volodymyr, Martin Sikor, Stanislav Kalinin, Dejana Mokranjac, Claus A. M. Seidel, and Don C. Lamb. 2012a. "Combining MFD and PIE for Accurate Single-Pair Förster Resonance Energy Transfer Measurements." *ChemPhysChem* 13 (4): 1060–78. https://doi.org/10.1002/cphc.201100822.

Kudryavtsev, Volodymyr, Martin Sikor, Stanislav Kalinin, Dejana Mokranjac, Claus A.M. Seidel, and Don C. Lamb. 2012b. "Combining MFD and PIE for Accurate Single-Pair Förster Resonance Energy Transfer Measurements." *ChemPhysChem* 13 (4): 1060–78. https://doi.org/10.1002/cphc.201100822.

Lagerström, Malin C, and Helgi B Schiöth. 2008. "Structural Diversity of G Protein-Coupled

Receptors and Significance for Drug Discovery." *Nature Reviews Drug Discovery* 7: 339. http://dx.doi.org/10.1038/nrd2518.

Latorraca, Naomi R., A. J. Venkatakrishnan, and Ron O. Dror. 2017. "GPCR Dynamics: Structures in Motion." *Chemical Reviews* 117 (1): 139–55. https://doi.org/10.1021/acs.chemrev.6b00177.

Laurence, Ted A., Xiangxu Kong, Marcus Jäger, and Shimon Weiss. 2005. "Probing Structural Heterogeneities and Fluctuations of Nucleic Acids and Denatured Proteins." *Proceedings of the National Academy of Sciences of the United States of America* 102 (48): 17348–53. https://doi.org/10.1073/pnas.0508584102.

Lee, Nam Ki, Achillefs N. Kapanidis, You Wang, Xavier Michalet, Jayanta Mukhopadhyay, Richard H. Ebright, and Shimon Weiss. 2005. "Accurate FRET Measurements within Single Diffusing Biomolecules Using Alternating-Laser Excitation." *Biophysical Journal* 88 (4): 2939–53. https://doi.org/10.1529/BIOPHYSJ.104.054114.

Lee, Sangbae, Soumadwip Ghosh, Suvamay Jana, Nathan Robertson, Christopher G. Tate, and Nagarajan Vaidehi. 2020. "How Do Branched Detergents Stabilize GPCRs in Micelles?" *Biochemistry* 59 (23): 2125–34. https://doi.org/10.1021/acs.biochem.0c00183.

Levitz, Joshua, Chris Habrian, Shashank Bharill, Zhu Fu, Reza Vafabakhsh, and Ehud Y. Isacoff. 2016. "Mechanism of Assembly and Cooperativity of Homomeric and Heteromeric Metabotropic Glutamate Receptors." *Neuron* 92 (1): 143–59. https://doi.org/10.1016/j.neuron.2016.08.036.

Marcaggi, P., H. Mutoh, D. Dimitrov, M. Beato, and T. Knopfel. 2009. "Optical Measurement of MGluR1 Conformational Changes Reveals Fast Activation, Slow Deactivation, and Sensitization." *Proceedings of the National Academy of Sciences* 106 (27): 11388–93. https://doi.org/10.1073/pnas.0901290106.

Müller, Barbara K, Evgeny Zaychikov, Christoph Bräuchle, Don C Lamb, B K Muller, and C Brauchle. 2005. "Pulsed Interleaved Excitation." *Biophysical Journal* 89 (5): 3508–22. https://doi.org/10.1529/biophysj.105.064766.

Nasrallah, Chady, Karine Rottier, Romain Marcellin, Vincent Compan, Joan Font, Amadeu Llebaria, Jean Philippe Pin, Jean Louis Banères, and Guillaume Lebon. 2018. "Direct Coupling of Detergent Purified Human MGlu5 Receptor to the Heterotrimeric G Proteins Gq and Gs." *Scientific Reports* 8 (1): 4407. https://doi.org/10.1038/s41598-018-22729-4.

Niswender, Colleen M., and P. Jeffrey Conn. 2010. "Metabotropic Glutamate Receptors: Physiology, Pharmacology, and Disease." *Annual Review of Pharmacology and Toxicology* 50 (1): 295–322. https://doi.org/10.1146/annurev.pharmtox.011008.145533.

O'Brien, Daniel E., Douglas M. Shaw, Hyekyung P. Cho, Alan J. Cross, Steven S. Wesolowski, Andrew S. Felts, Jonas Bergare, et al. 2018. "Differential Pharmacology and Binding of MGlu 2 Receptor Allosteric Modulators." *Molecular Pharmacology* 93 (5): 526–40. https://doi.org/10.1124/mol.117.110114.

Olofsson, Linnea, Suren Felekyan, Etienne Doumazane, Pauline Scholler, Ludovic Fabre, Jurriaan M Zwier, Philippe Rondard, Claus A M Seidel, Jean-Philippe Pin, and Emmanuel Margeat. 2014. "Fine Tuning of Sub-Millisecond Conformational Dynamics Controls Metabotropic Glutamate Receptors Agonist Efficacy." *Nature Communications* 5: 5206. http://dx.doi.org/10.1038/ncomms6206.

Olofsson, Linnea, and Emmanuel Margeat. 2013. "Pulsed Interleaved Excitation Fluorescence Spectroscopy with a Supercontinuum Source." *Optics Express* 21 (3): 3370–78. https://doi.org/10.1364/OE.21.003370.

Pin, Jean-Philippe, and Bernhard Bettler. 2016. "Organization and Functions of MGlu and GABAB Receptor Complexes." *Nature* 540 (7631): 60–68. https://doi.org/10.1038/nature20566.

Scholler, Pauline, David Moreno-Delgado, Nathalie Lecat-Guillet, Etienne Doumazane, Carine Monnier, Fabienne Charrier-Savournin, Ludovic Fabre, et al. 2017. "HTS-Compatible FRET-Based Conformational Sensors Clarify Membrane Receptor Activation." *Nature Chemical Biology* 13 (4): 372–80. https://doi.org/10.1038/nchembio.2286.

Schrage, R, A De Min, K Hochheiser, E Kostenis, and K Mohr. 2016. "Superagonism at G Protein-

Coupled Receptors and Beyond." *British Journal of Pharmacology* 173 (20): 3018–27. https://doi.org/10.1111/bph.13278.

Schrimpf, Waldemar, Anders Barth, Jelle Hendrix, and Don C. Lamb. 2018. "PAM: A Framework for Integrated Analysis of Imaging, Single-Molecule, and Ensemble Fluorescence Data." *Biophysical Journal* 114 (7): 1518–28. https://doi.org/10.1016/j.bpj.2018.02.035.

Selvin, Paul R. 2002. "Principles and Biophysical Applications of Lanthanide-Based Probes." *Annual Review of Biophysics and Biomolecular Structure*. Annu Rev Biophys Biomol Struct. https://doi.org/10.1146/annurev.biophys.31.101101.140927.

Sisamakis, Evangelos, Alessandro Valeri, Stanislav Kalinin, Paul J. Rothwell, and Claus A.M. Seidel. 2010. "Accurate Single-Molecule FRET Studies Using Multiparameter Fluorescence Detection." In *Methods in Enzymology*, 475:455–514. Academic Press Inc. https://doi.org/10.1016/S0076-6879(10)75018-7.

Strohman, M. J., S. Maeda, D. Hilger, M. Masureel, Y. Du, and B. K. Kobilka. 2019. "Local Membrane Charge Regulates B2 Adrenergic Receptor Coupling to Gi3." *Nature Communications* 10 (1): 1–10. https://doi.org/10.1038/s41467-019-10108-0.

Thompson, Aaron A., Jeffrey J. Liu, Eugene Chun, Daniel Wacker, Huixian Wu, Vadim Cherezov, and Raymond C. Stevens. 2011. "GPCR Stabilization Using the Bicelle-like Architecture of Mixed Sterol-Detergent Micelles." *Methods* 55 (4): 310–17. https://doi.org/10.1016/j.ymeth.2011.10.011.

Tian, He, Alexandre Furstenberg, and Thomas Huber. 2017. "Labeling and Single-Molecule Methods to Monitor G Proteincoupled Receptor Dynamics." *Chemical Reviews* 117 (1): 186–245. https://doi.org/10.1021/acs.chemrev.6b00084.

Vafabakhsh, Reza, Joshua Levitz, and Ehud Y Isacoff. 2015. "Conformational Dynamics of a Class C G-Protein-Coupled Receptor." *Nature* 524 (7566): 497–501. https://doi.org/10.1038/nature14679.

Weis, William I, and Brian K Kobilka. 2018. "The Molecular Basis of G Protein-Coupled Receptor

Activation." *Annual Review of Biochemistry*. https://doi.org/10.1146/annurev-biochem-060614-033910.

Wu, Huixian, Chong Wang, Karen J Gregory, Gye Won Han, Hyekyung P Cho, Yan Xia, Colleen M Niswender, et al. 2014. "Structure of a Class C GPCR Metabotropic Glutamate Receptor 1 Bound to an Allosteric Modulator." *Science (New York, N.Y.)* 344 (6179): 58–64. https://doi.org/10.1126/science.1249489.

Xue, Li, Xavier Rovira, Pauline Scholler, Han Zhao, Jianfeng Liu, Jean-Philippe Pin, and Philippe Rondard. 2015. "Major Ligand-Induced Rearrangement of the Heptahelical Domain Interface in a GPCR Dimer." *Nature Chemical Biology* 11 (2): 134–40. https://doi.org/10.1038/nchembio.1711.

Xue, Li, Qian Sun, Han Zhao, Xavier Rovira, Siyu Gai, Qianwen He, Jean-Philippe Pin, Jianfeng Liu, and Philippe Rondard. 2019. "Rearrangement of the Transmembrane Domain Interfaces Associated with the Activation of a GPCR Hetero-Oligomer." *Nature Communications* 10 (1): 2765. https://doi.org/10.1038/s41467-019-10834-5.

Zhang, Jinyi, Lu Qu, Lijie Wu, Xiaomeng Tang, Feng Luo, Weixiu Xu, Yueming Xu, Zhi Jie Liu, and Tian Hua. 2020. "Structural Insights into the Activation Initiation of Full-Length MGlu1." *Protein and Cell*. Higher Education Press Limited Company. https://doi.org/10.1007/s13238-020-00808-5.